



HAL
open science

Numerical simulations of combined size effects acting on an open-hole laminated composite plate under tension

Joel Serra, Christophe Bouvet, Prajwal Karinja Haridas, Léon Ratsifandrihana

► To cite this version:

Joel Serra, Christophe Bouvet, Prajwal Karinja Haridas, Léon Ratsifandrihana. Numerical simulations of combined size effects acting on an open-hole laminated composite plate under tension. *Journal of Composite Materials*, In press, 10.1177/00219983221139791 . hal-03897090

HAL Id: hal-03897090

<https://hal.science/hal-03897090v1>

Submitted on 13 Dec 2022

HAL is a multi-disciplinary open access archive for the deposit and dissemination of scientific research documents, whether they are published or not. The documents may come from teaching and research institutions in France or abroad, or from public or private research centers.

L'archive ouverte pluridisciplinaire **HAL**, est destinée au dépôt et à la diffusion de documents scientifiques de niveau recherche, publiés ou non, émanant des établissements d'enseignement et de recherche français ou étrangers, des laboratoires publics ou privés.



Numerical simulations of combined size effects acting on an open-hole laminated composite plate under tension

Journal:	<i>Journal of Composite Materials</i>
Manuscript ID	JCM-22-0471.R1
Manuscript Type:	Original Manuscript
Date Submitted by the Author:	27-Sep-2022
Complete List of Authors:	Serra, Joel; ISAE-SUPAERO; Institut Clement Ader bouvet, christophe; ISAE-SUPAERO; Institut Clement Ader, KARINJA HARIDAS, Prajwal; ISAE-SUPAERO; Institut Clement Ader Ratsifandrihana, Leon; Segula Technologies
Keywords:	Size effect, Open-hole tensile test, Thickness effect, Blocked plies, Discrete Ply Modeling, Finite Element Model
Abstract:	<p>Numerical and experimental research programs have been carried out to investigate the effect of scaling on the tensile strength of notched composites. This paper presents a computational study of scaled open-hole tensile tests using the Discrete Ply Modeling (DPM) method. This finite element model is discrete, and only a small number of parameters are required from experimental characterization tests. Experimental and numerical strength values are compared here, and reveal that DPM simulations tend to slightly overestimate strength values, with an average discrepancy of 9.7%. However, DPM Results show that such modeling simulates both the reduction in strength when specimen size is increased for sublaminar level scaled specimens, where failure is fiber dominated, and the increase in strength when specimen size is increased for ply level scaled specimens, where failure is delamination dominated. In all cases, increasing the total thickness of the specimen leads to a decrease in strength and this effect is dominant over the effect of increasing hole diameter. As well as the variation in strength, three distinct failure mechanisms are observed: fiber failure with extensive matrix damage (pull-out failure), fiber failure with little or no matrix damage (brittle failure) and delamination failure. Comparisons with experiments demonstrate that tensile strengths, damage propagation scenarios and failure patterns are predicted with acceptable accuracy.</p>

1
2
3
4
5
6
7
8
9
10
11
12
13
14
15
16
17
18
19
20
21
22
23
24
25
26
27
28
29
30
31
32
33
34
35
36
37
38
39
40
41
42
43
44
45
46
47
48
49
50
51
52
53
54
55
56
57
58
59
60



Numerical simulations of combined size effects acting on an open-hole laminated composite plate under tension

J. Serra¹, C. Bouvet^{1,*}, P. Karinja Haridas¹ and L. Ratsifandrihana²

¹Université de Toulouse, Institut Clément Ader, ISAE-SUPAERO – UPS – IMT Mines Albi – INSA

Toulouse, FRANCE

²SEGULA Aerospace and Defence

Colomiers, FRANCE

*Corresponding author: christophe.bouvet@isae-supero.fr

Abstract:

Numerical and experimental research programs have been carried out to investigate the effect of scaling on the tensile strength of notched composites. This paper presents a computational study of scaled open-hole tensile tests using the Discrete Ply Modeling (DPM) method. This finite element model is discrete, and **only a small number of parameters** are required **from experimental characterization tests**. Experimental and numerical strength values are compared here, and reveal that **DPM simulations tend to slightly overestimate strength values, with an average discrepancy of 9.7%. However**, DPM Results show that such modeling simulates **both** the reduction in strength when specimen size is increased for sublaminar level scaled specimens, where failure is fiber dominated, **and the increase in strength when specimen size is increased for ply level scaled specimens, where failure is delamination dominated**. In all cases, increasing **the total thickness of the specimen** leads to a decrease in strength and this effect is dominant over the effect of increasing hole diameter. As well as the variation in strength, three distinct failure mechanisms are observed: fiber failure with extensive matrix damage (pull-out failure), fiber failure with little or no matrix damage (brittle failure) and delamination failure. Comparisons with experiments demonstrate that tensile strengths, damage propagation scenarios and failure patterns are predicted with acceptable accuracy.

Keywords: Size effect; Open-hole tensile test; Thickness effect; Blocked plies; Discrete Ply Modeling

I. Introduction

Composite materials have become indispensable in the aerospace and astronautics sectors. Aircraft that use composite structures have many parts containing holes or different cut-outs that induce stress concentrations and reduce the strength of the part. When they are subjected to tensile loading, damage and failure mechanisms around these holes/cut-outs are magnified because of stress concentrations. Notched strength is therefore one of the most important design drivers for composite structures [1]. The mechanical performance of open-hole composite laminates depends on many factors, such as the size and thickness of the laminate; the hole size and its location; the plies orientations and the machining quality. Before real composite structures are tested, the effects of holes are studied on coupons 10-100 times smaller. Understanding the associated scaling effects is therefore of the utmost importance. Since the discovery of these scaling phenomena by Leonardo da Vinci in the early 1500s [2], substantial amounts of research have been devoted to them but deep understanding is still lacking.

To explore the physical causes of scaling effect, numerous experiments have been conducted [3]–[5]. Size effect can occur at different levels [6]. At the structural level, when thin plies are used, it has been proven that the strength of notched composite laminates decreases when the notch size increases. At the material level, the “in situ” effect has been detected and is influenced by the ply thickness. Wisnom et al. [4] have analyzed this phenomenon on quasi-isotropic specimens.

The “hole size effect” has been studied at the structural level. In this configuration, increasing hole diameter leads to a decrease in the strength of a laminate. The presence of non-critical ply-level damage, such as matrix failure, delamination, fiber splitting and fiber fracture in the vicinity of the hole blunts the stress concentration [7]. The strength difference between small and large specimens [8] is explained by the extent of the “fracture process zone”, which is relatively independent of the size of the specimen.

Using a sublaminar level scaling method, Harris and Morris [9] investigated the effect of an increase in the total thickness of a laminate with a constant ply thickness. They observed that increasing thickness in quasi-isotropic laminates led to a decrease in strength because the damage prior to failure was confined to a boundary close to the surface, so thicker laminate experienced less stress redistribution throughout the laminate.

Using a ply-level scaling method, Vaidya et al. [10] increased the thickness of their laminates. They observed similar fracture toughness values and similar amounts of sub-critical damage during loading for quasi-isotropic $[0_n/90_n/-45_n/45_n]_s$ laminates with $n = 1$ and $n = 2$. However, with $n = 4$, the failure mechanism changed from fiber failure to delamination failure along the 0/90 interface, resulting in the increase of sub-critical damage, accompanied by a marked decrease in fracture toughness.

1 The influence of stacking sequence and hole diameter on the notched strength of a laminate was
2 also investigated by Lagace [11]. He used a constant specimen width that gave varying stress
3 concentration across the width. He found that increasing hole diameter led to a change in fracture
4 mechanism, from a matrix-dominated to a fiber-dominated failure, for $[0/90_2]_s$ laminates. This was
5 caused by the fact that increasing the hole-radius-to-laminate-thickness ratio led to a decrease in
6 interlaminar stresses in the region around the hole boundary. Laminates with little or no delamination
7 showed linear stress-strain curves up to failure whereas those with large amounts of delamination
8 prior to failure exhibited large non-linearities. Chang et al. [12] found that damage propagates from a
9 circular hole via matrix failure in the off-axis plies.

10 Preliminary sizing solutions for notched composites are mainly based on semi-empirical
11 analytical models for predicting notched strength, such as the point stress or the average stress
12 models [13], [14]. An extensive review of these technics has been provided by Awerbuch and
13 Madhukar [15]. Whitney and Nuismer [13] developed two related criteria based on normal stress
14 distribution to predict the residual strength of laminated composites containing a through-the-
15 thickness discontinuity. They presented specific examples for a circular hole in quasi-isotropic
16 material and for a notch in $[0/\pm 45_2]_s$ glass/epoxy laminated plates. In both cases, comparison of
17 experimental data and theory showed good correlation. Various researchers have developed stress-
18 based models, with varying levels of complexity and of success [8], [16]–[23]. Fast semi-analytical
19 and numerical methods [24]–[27] have given good agreement between experimental data and
20 numerical predictions for quasi isotropic laminates. However, they do not take the influence of the
21 stacking sequence into account since they consider that strain is constant within the laminate
22 thickness [28]. A more complete numerical model is therefore needed to predict the physics
23 associated with failure phenomena (delamination and transverse cracks).

24 Many models have been proposed to fit experimental data [4], [29]–[35]. They can be classified
25 according to their level of discretization [33], from the whole continuum model without any
26 interfaces to the most discretized type of model, where the three most important types of damage
27 (fiber failure, matrix cracking and delamination) are all represented through interfaces. To correctly
28 model matrix cracks and their interaction with delamination, discrete elements seem necessary [35].
29 The best way to represent strong discontinuities, i.e. matrix cracking, should be the discrete crack
30 methods. Numerical studies on open-hole laminate composites, conducted by Hallett et al. [4] and
31 Jiang et al. [36] using a simplified mesh coupled with a strong simplification of the hole geometry,
32 confirm these assumptions. Swindeman et al. [37] established a regularized X-FEM (Extended Finite
33 Element Model) with a predefined minimum crack spacing. However, as the maximum number of
34 representable cracks per ply is in strong correlation with the number of degrees of freedom, its use is
35 limited. The model did not include fiber failure, but was able to capture matrix cracks and two load
36 drops due to excessive delamination, captured by the cohesive zone method. Chen et al. [38] applied
37 the floating node method and enriched 3D cohesive element to improve the connectivity between the

plies and interlayer. Bao and Liu [39] used surface-based cohesive contact for major split cracks tangential to the hole as well as delamination. The distributed matrix cracks appeared to be captured by continuum damage mechanics. Higuchi et al. [40] presented a coupled X-FEM/CZM (Cohesive Zone Model) approach where fiber failure was not modeled. A predefined crack spacing was used to model all potential matrix cracks, and delamination by interface elements. Joosten et al. [41] developed a model in which cohesive elements are used for all failure modes, i.e. fiber, matrix and interface failure. Lu et al. [42] used an adaptive discrete-smear crack model, where the critical discrete matrix cracks were captured by the floating node method with a crack alignment algorithm. To capture the interaction between splitting and delamination, delamination was modeled with separable cohesive elements. The model was able to predict major and minor distributed cracks and delamination migration.

Numerous models have been created to simulate open-hole laminate composite behavior but few have been used to model size effects. The Discrete Ply Model (DPM) used in this paper employs cohesive interfaces to model matrix failure and delamination, and 3D volume elements to predict fiber failure. It was initiated by Bouvet et al. for modeling low velocity impacts in composite panels [43], and afterwards enhanced to capture permanent indentation [44] and to simulate compression after impact [45]. The use of interfaces connected by a specific mesh makes the coupling between the intra- and inter-laminar damage natural. The DPM has also been used to represent pull-through cases [46] where the effects of splitting on the load redistribution were correctly predicted. In addition, after a modification of the hole contour mesh, the DPM has also been able to predict notched strength, failure scenarios and failure patterns on different stacking sequences [47] and a first study of the scaling effect in notched composites has been performed [48].

To the knowledge of the authors, the only numerical work on a wide range of laminate thicknesses, hole diameters and stacking sequences on an open hole tension configuration has been performed by Hallet et al. [7]. There are three main differences between the approach developed by Hallet and that of the work presented here (DPM). First, in Hallet et al.'s approach, the fiber failure is simulated using a stress criterion based on Weibull statistics. Calibration is therefore needed to extract the two parameters of the Weibull law. In the DPM approach, the fiber failure is only determined by "physical parameters": the failure strain and the critical energy release rate. Second, the locations of the matrix cracks are explicitly determined from experimental observations in [7], whereas the DPM meshing strategy situates cohesive interfaces everywhere in order to have a "blind approach" and to develop a more generic model. Third, the numerical predictions [7] are not able to distinguish pull-out failure from brittle failure, whereas the DPM results predict them satisfactorily.

In this paper, the DPM is used to simulate 18 configurations tested experimentally by Green et al. [1]. The experimental strength results are compared to numerical ones. A thorough investigation on the origin of scaling effects on the strength of notched composites is performed. The

1 following section gives details of the experimental procedure. Then, the DPM modeling strategy is
2 detailed and the results are compared with experimental data. **The DPM has been used as a**
3 **prospective tool to establish charts for engineers to help select the best stacking sequence to use**
4 **for a given laminate thickness/ hole diameter combination.**
5
6
7
8
9
10
11
12
13
14
15
16
17
18
19
20
21
22
23
24
25
26
27
28
29
30
31
32
33
34
35
36
37
38
39
40
41
42
43
44
45
46
47
48
49
50
51
52
53
54
55
56
57
58
59
60

For Peer Review

II. Experimental procedure

This paper presents a numerical investigation of the experimental data from research carried out by Green et al. [1]. They performed open hole tensile tests on IM7/8552 carbon fiber/epoxy quasi-isotropic laminates manufactured from prepegs supplied by Hexcel. The nominal ply thickness was 0.125 mm. Laminates were autoclave cured according to Hexcel's recommended cure cycle [49], and specimens were cut from these using a water-cooled diamond saw. The holes were drilled with tungsten carbide drill bits, with the drill speed scaled according to the hole diameter so that a constant cutting speed was used. Specimens with a central circular hole were tested in quasi-static tension. Constant length to hole diameter (L/D) and width to hole diameter (W/D) ratios were used, as shown in Figure 1. Six specimens for each condition were loaded to failure. A nominal strain rate of 0.78%/min was used, which equates to using constant displacement rates of 0.5, 1, 2 and 4 mm/min for hole diameters of 3.175, 6.35, 12.7 and 25.4 mm, respectively. Many of the tests were recorded with a video camera using a high magnification lens, so that the ply-level damage during the test could be determined.

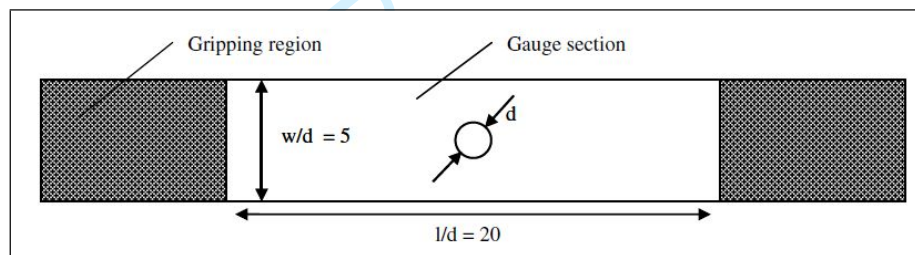


Figure 1. Specimen geometry [1]

The stacking sequence of the laminate used was $[45_m/90_m/-45_m/0_m]_n s$ with 0° being the direction of the applied load [1]. The subscripts m and n refer to the number of plies of each orientation, representing two different ways of increasing the thickness of the laminate. Those different ways are represented in Figure 2.

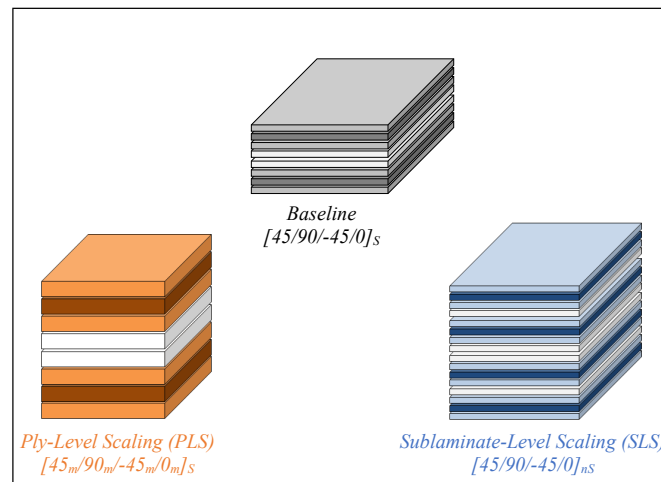


Figure 2. Different ways of increasing laminate thickness (adapted from [1])

<http://mc.manuscriptcentral.com/jcm>

Increasing m increases the effective ply thickness, i.e. it increases the number of plies of the same orientation that are blocked together. From here on, this is referred to as ply-level scaling, and noted PLS. Increasing n increases the laminate thickness by increasing the number of sublaminates but keeps the ply thickness constant. From here on, this is referred to as sublaminating-level scaling, and noted SLS. Three different scaling routines were used: one dimensional (1D), two-dimensional (2D) and three-dimensional scaling (3D), as presented on the testing program matrix of Table 1.

t (mm)	<i>Sublaminating-level Scaling</i>				<i>Ply-level Scaling</i>			
	<i>Hole diameter (mm)</i>				<i>Hole diameter (mm)</i>			
	3.175	6.35	12.7	25.4	3.175	6.35	12.7	25.4
1								
2	1D							
4			2D					
8								


 Configuration tested

Table 1. Testing program matrix [1]

One-dimensional scaling consists in keeping the hole diameter constant and increasing only the thickness of the laminate. In the case of two-dimensional scaling, the thickness remains constant and the in-plane dimensions (hole diameter, and hence width and length) are increased. Three-dimensional scaling consists in increasing the hole diameter while increasing the thickness of the laminate. As described by Green et al. [1], failure was taken as the first significant load drop on the load-displacement curve (greater than 5%). Table 2 and Table 3 summarize the values of failure stresses obtained by numerical simulation by DPM (presented in the next section) and experimental results from Green et al. [1], covering both laminates with all plies blocked together and multiple sublaminates of single plies. **Only the failure stresses are given, without the experimental stress/strain curves. Examination of the specimens post failure showed three distinct types of failure mechanisms [1]. These have been termed pull out (fiber-dominated failure with extensive sub-critical damage - Figure 3/top left), brittle (fiber-dominated failure with little subcritical damage - Figure 3/top right) and delamination (matrix-dominated - Figure 3/bottom) type failures. The configurations for which they occurred are shown in Table 4.**

SLS	<i>Hole Diameter (mm)</i>							
	3.175		6.35		12.7		25.4	
<i>thickness (mm)</i>	<i>DPM</i>	<i>Exp</i>	<i>DPM</i>	<i>Exp</i>	<i>DPM</i>	<i>Exp</i>	<i>DPM</i>	<i>Exp</i>
1	594	570						
2	544	500	484	438				
4	485	478	464	433	405	374	371	331
8	495	476					326	332

Table 2. Numerical vs experimental average failure stress (in MPa) of sublaminating-level scaled specimens (exp. results from [1])

PLS thickness (mm)	Hole Diameter (mm)							
	3.175		6.35		12.7		25.4	
	DPM	Exp	DPM	Exp	DPM	Exp	DPM	Exp
1	594	570						
2	451	396	451	498				
4	297	275	350	285	396	362	427	417
8	225	202					314	232

Table 3. Numerical vs experimental average failure stress (in MPa) of ply-level scaled specimens (exp. results from [1])

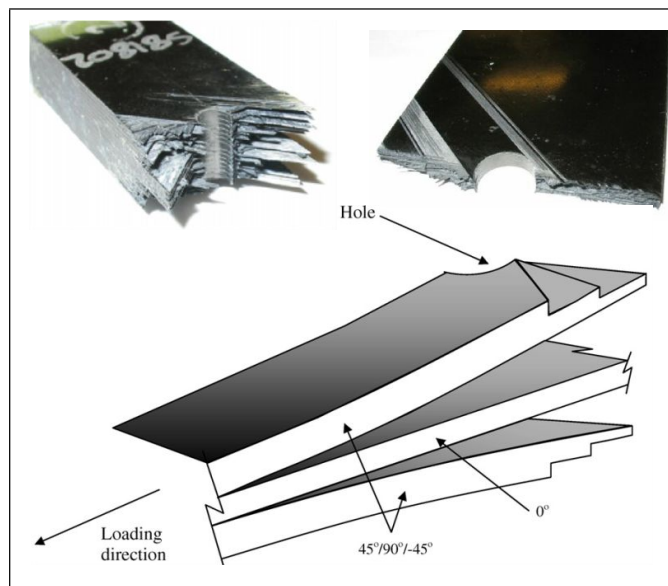


Figure 3. Top - Photographs of pull-out failure (left) and brittle failure (right)
Bottom – Schematic diagram of delamination failure [1]

t (mm)	Sublaminates-level Scaling				Ply-level Scaling			
	Hole diameter (mm)				Hole diameter (mm)			
	3.175	6.35	12.7	25.4	3.175	6.35	12.7	25.4
1	Diagonal Hatching				Diagonal Hatching			
2	Diagonal Hatching	Diagonal Hatching			Diagonal Hatching	Diagonal Hatching		
4	Diagonal Hatching	Diagonal Hatching	Grey	Grey	Black	Black	Black	Black
8	Diagonal Hatching			Grey	Black	Black	Black	Black




 Pull-out failure
 Brittle type failure
 Delamination type failure

Table 4. Failure mechanisms in testing program [1]

III. Numerical modeling

The Discrete Ply Model (DPM) is a finite element model developed in Abaqus/Explicit. It takes the three major failure modes in composites into account: fiber failure in intra-ply, matrix cracking in intra-ply, and delamination in inter-ply, as shown in Figure 4. **The DPM has been successfully used to simulate the behavior of laminated composite under various loadings: low velocity impact [43], [44], compression after impact [45], fastener pull-through [46,], open hole [47], [48] and notched [50] tension, as well as multiaxial loadings on larger notched specimens [51].** The mesh consists of 3D volume elements (C3D8) used to model fiber fracture, separated by zero-thickness cohesive elements (COH3D8) to represent delamination and matrix cracking. **The behavior of these three types of elements was implemented using a user-defined VUMAT subroutine.**

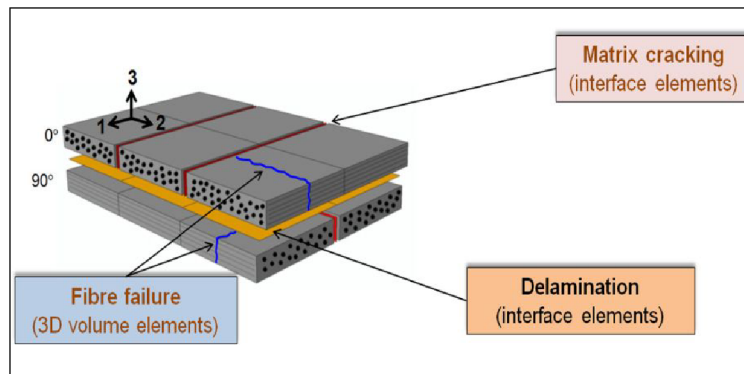


Figure 4. Discrete Ply Model damage failure modes [33]

The mesh construction from previous work is displayed in Figure 5: there were four (initially coincident) nodes for each geometrical vertex. Two of them were used to model matrix cracking of the lower ply and the other two to model the matrix cracking of the upper ply. Matrix cracking/delamination coupling was achieved naturally as the two pairs of nodes were connected by delamination elements. In order to make all the nodes coincident, it was necessary to use parallelogram-shaped elements for -45° and 45° plies, while 0° and 90° plies were meshed in a square shape (Figure 5).

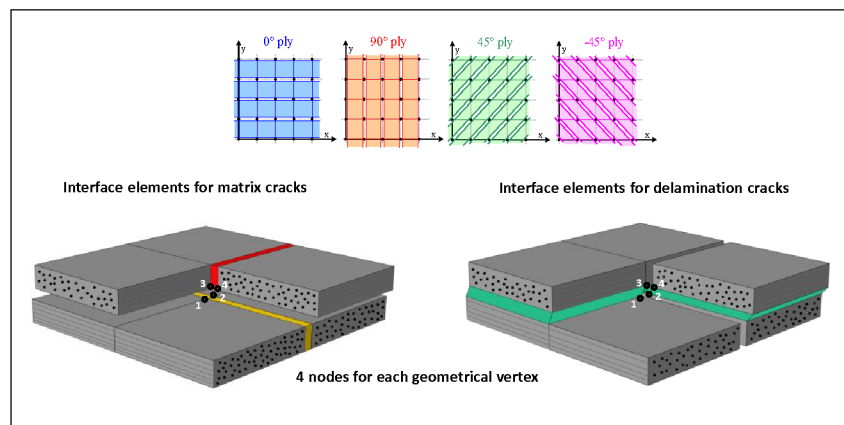


Figure 5. Mesh specificities of the Discrete Ply Model [33]

<http://mc.manuscriptcentral.com/jcm>

For each simulation, the element size was kept constant at 0.250 mm, i.e. twice the thickness of a single ply. This choice was justified by experimental tests, which showed that, within a ply, two matrix cracks tended to be separated by at least 1.5–2 times the ply thickness (Figure 6). Hence, refining the mesh would not be in accordance with the physical reality, and using a rougher mesh (increasing the distance between two matrix cracks) would lead to more numerically unstable, high-aspect-ratio volume elements. Li and Chen [52] determined the minimum distance between two matrix cracks numerically for HS300/ET223 and T300/NY9200Z composite laminates. The results showed a factor of 1.53 and 1.60 between the minimum distances separating transverse cracks and the ply thickness, which confirmed the experimental observations. Saturation crack distance was substantially more affected by the thickness of the cracked ply than by the stiffness of neighbouring plies.

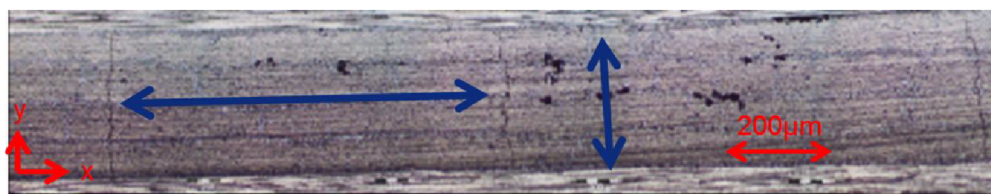


Figure 6. Matrix cracks within a 90° ply from a T700/M21 laminate ([0/9040/0]s) under three point bending [48]

For the four diameters simulated, the hole meshing technique consisted in using a grid scheme discretization and projecting the nodes inside the circular holes onto the contour of the hole [47]. A few elements, excessively distorted, would lead to numerical divergence and were consequently removed [47], [48] but the circular shapes were correctly described (Figure 7).

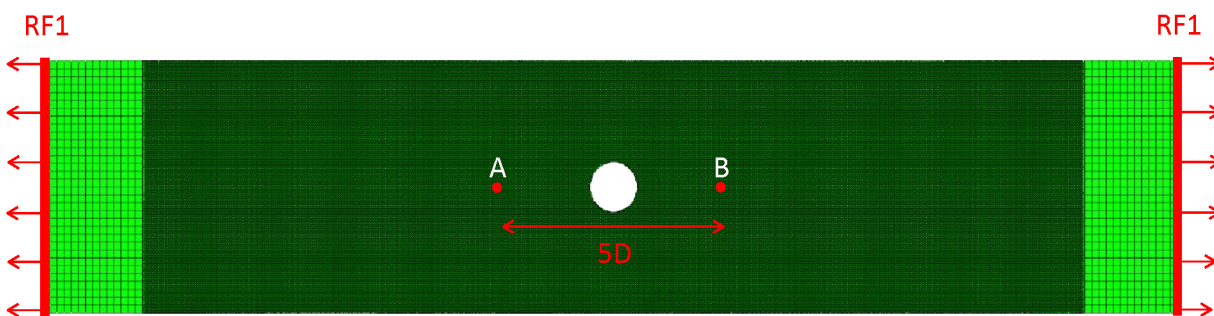


Figure 7. Finite element model and evaluation of the average stress and average strain

The reaction force named *RF1* on set 1 (Figure 7) is the reaction due to the applied displacement. To obtain the stress-strain curves, this value is used to calculate the average stress, σ , as:

$$\sigma = \frac{RF1}{width \times thickness} \quad (1)$$

The variation of displacement, named Δu , between point A and B is also noted and allows the average strain, ε , to be calculated as:

$$\varepsilon = \frac{\Delta u}{AB} = \frac{u_B - u_A}{AB} \quad (2)$$

with u_B (u_A) the displacement of the point A (B) and AB the initial distance between A and B . The initial distance between the points A and B was chosen equal to $5D$ in order to evaluate the effect of the hole.

The numerical displacement speed was selected so as to ensure that the corresponding additional energy was negligible, while keeping a reasonable calculation time by using multiple CPUs in parallel. A total calculation time of 5 ms was used for the “Small” specimens and of 10 ms for the larger sizes. To ensure that changes in the calculation time and consequent increases in the inertial forces do not alter the solution significantly, a calculation was performed with a numerical displacement speed 4 times less than the initial one and showed similar results. Computation time varied between 30 min (36 CPUs) for the “Small” specimens with about 100,000 elements and 60 h (72 CPUs) for the largest specimens with about 5,000,000 elements. The DPM uses a small number of parameters that are all provided by experimental tests [43-48]; no coupling parameter is required.

Density		1580 kg/m ³
Elastic Properties		
E_1^T	Tensile Young's modulus in fibre direction	161 GPa
E_1^C	Compressive Young's modulus in fibre direction	140 GPa
E_2	Transverse Young's modulus	11.4 GPa
ν_{12}	Poisson ratio	0.3
G_{12}	Shear modulus	5.17 GPa
Matrix cracking		
σ_t^f	Transverse tensile strength	80 MPa
σ_c^f	Transverse compressive strength	-150 MPa
τ_{lt}^f	In-plane shear strength	90 MPa
Fiber failure		
ε_0^T	Tensile strain in fibre direction at damage initiation	1.58%
ε_0^C	Compressive strain in fibre direction at damage initiation	-1.23%
$G_{Ic}^{fibre,t}$	Fracture toughness for mode I in traction	196 N/mm
$G_{Ic}^{fibre,c}$	Fracture toughness for mode I in compression	102 N/mm
Delamination		
G_{Ic}^{del}	Interface fracture toughness for opening mode (I)	0.20 N/mm
G_{IIc}^{del}	Interface fracture toughness for shear mode (II & III)	1.0 N/mm

Table 5. Material properties of the IM7/8552 carbon epoxy ply (0.125 mm)

<http://mc.manuscriptcentral.com/jcm>

1. Modeling of matrix cracking

As presented in Figure 4, the matrix cracking is taken into account using vertical zero-thickness interface elements between 2 consecutive volume elements. The failure criterion is calculated in the volume elements neighboring the interface elements, to avoid stress concentration. The stiffness of the interface (initially 10^6 MPa/mm) is set to zero if the Hashin criterion (1) is reached in either of the neighboring volume elements:

$$\left[\frac{\langle \sigma_t \rangle^+}{\langle \sigma_t^f \rangle} \right]^2 + \frac{\tau_{lt}^2 + \tau_{tz}^2}{(\tau_t^f)^2} \leq 1 \quad (3)$$

where σ_t is the transverse stress, τ_{lt} and τ_{tz} are the shear stresses in the (lt) and (tz) planes, σ_t^f is the transverse failure stress and τ_t^f is the shear failure stress of the ply.

When interface elements are used to simulate matrix cracking, as only through-the-ply cracks are taken into account in this method, diffuse damage is not modeled. The supporting hypothesis is that in a thin ply, a matrix crack propagates fast and therefore diffuse damage should not be represented.

2. Modeling of delamination

Delamination is modeled using cohesive interfaces like matrix cracking (Figure 4). Unlike for the matrix cracking, in the case of delamination, energy is dissipated, **since, if we were to use an energy based criterion for matrix cracking, the energy dissipated would be dependent on mesh density.** However, energy spent in matrix cracking is still taken into account: when the critical energy release rate for delamination is measured, it encompasses delamination energy and most of the energy dissipated through matrix cracking as the classical tests used to evaluate the fracture toughness (Double Cantilever Beam or End Notched Flexure tests) include several types of damage. **The energy dissipated through matrix cracking is therefore not taken into account in the matrix crack behavior law but rather in the delamination one.**

For the present discrete modelling, even if there is no parameter coupling delamination and matrix cracking, the discontinuity still allows this interaction to take place. Delamination normally occurs between differently oriented plies. It was therefore simulated in interface elements, and joining nodes of lower and upper volume ply elements (Figure 5). Mode I was in the thickness direction normal to the delamination plane, while mode II and mode III were in the in-plane direction. A mode I delamination is initiated when the distance between nodes reaches a critical distance d_I^0 , then degradation of the stiffness in mode I is established, and ends when the critical energy release rate in delamination in mode I, G_{Ic} , is dissipated (**Figure 8-Left**). **Through the energy dissipation of fracture mechanics, the criterion of delamination was simulated as**

linear coupling in three modes, based on a power law criterion of mixed-mode delamination propagation with the energy release rate (Figure 8- Right):

$$\frac{G_I}{G_{Ic}} + \frac{G_{II}}{G_{IIc}} + \frac{G_{III}}{G_{IIIc}} = 1 \quad (4)$$

G_{Ic} , G_{IIc} and G_{IIIc} are the critical energy release rates in modes I, II and III respectively. The modes II and III are considered equal ($G_{IIc} = G_{IIIc}$).

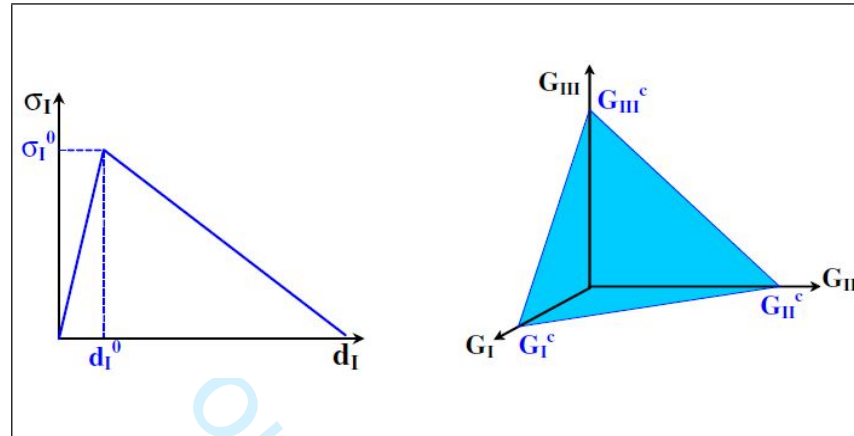


Figure 8. DPM delamination behavior law [33]

Left – Pure Mode I, Right – Mixed mode

3. Modeling of fiber failure

Fiber failure was modeled continuously as described in Figure 9: failure is initiated when the fiber strain reaches the failure strain ε_0^T and is propagated using the critical energy release rate G_{Ic}^f . The fiber continues to lengthen until consistent energy ($S \cdot G_{Ic}^f$) has been dissipated. The stiffness of the affected volume elements is gradually reduced until fiber strain reaches ε_1^T :

$$\int_V \left(\int_0^{\varepsilon_1^T} \sigma_l \cdot d\varepsilon_l \right) \cdot dV = S \cdot G_{Ic}^f \quad (4)$$

where $\sigma_l(\varepsilon_l)$ is the longitudinal stress (strain), $V(S)$ is the volume (section) of the element, ε_1^T is the strain of total degradation of the fiber stiffness (Figure 9), and G_{Ic}^f is the critical energy release rate in opening mode in the fiber direction. First order volume elements (C3D8) were chosen, as two nodes along the thickness direction of the ply are sufficient to describe linear strain variation within the element.

In order to be able to dissipate the critical energy released due to fiber failure fracture per unit area of crack, a communication law between the 8 integration points was used within each element to determine the average energy release restitution rate (over 8 integration points) and the different ε_i^T (with i the integration point number). The black line in Figure 9 represents the stress/strain curve evolution of the first integration point that reaches ε_0^T . The 7 grey lines display the stress/strain curve evolution of the other 7 integration points. Independently of the

element length, constant energy is released per unit area. The characteristic length used in the model, which is the volume element length, ensures the mesh independency [2], [3].

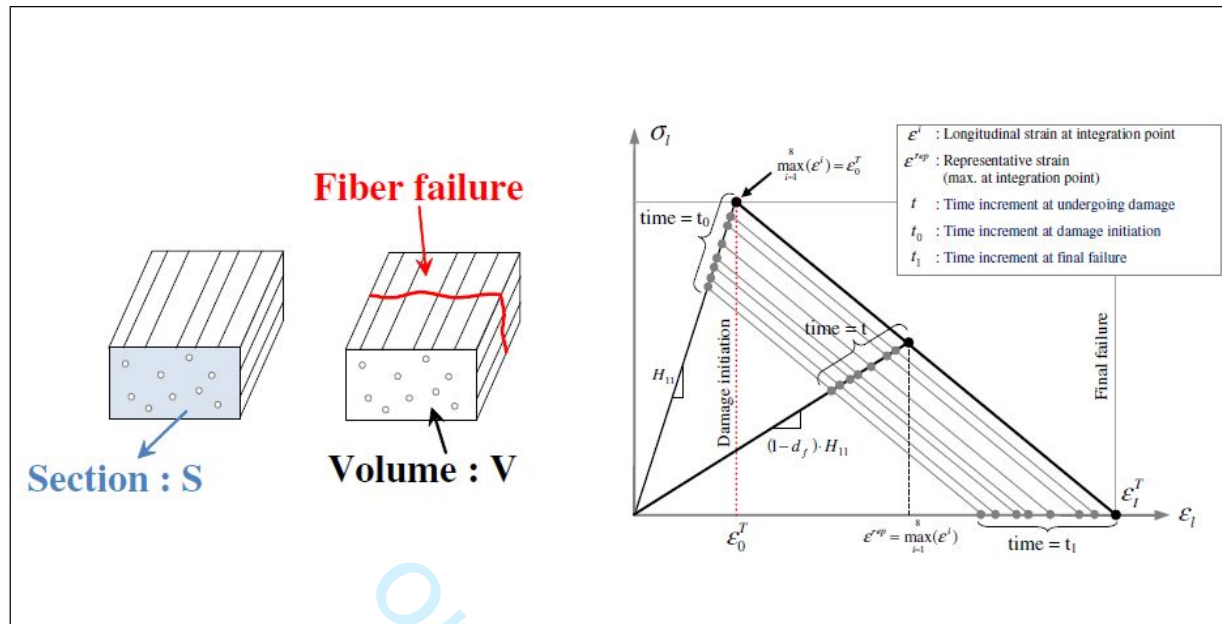


Figure 9. Discrete Ply Modeling of fiber failure [33]

IV. Results

It has been well-known since the seventies that, on composite laminates, increasing the size of a specimen with constant width-to-diameter ratio reduces the strength. With the ply-level scaling method, increasing the number of plies blocked together caused a larger drop in strength than in the sublaminates-level scaling method, due to interlaminar constraints.

1. Baseline specimen

Before analyzing the results of the two different ways of increasing the thickness of the laminate used, it seems important to see how damage occurs on the baseline specimen. The baseline configuration can be considered to be of both PLS and SLS type.

Regarding the baseline specimen ($t=1\text{ mm}$), delamination occurs at higher stress than for thicker specimens ($t=2\text{ mm}$, $t=4\text{ mm}$, $t=8\text{ mm}$) and the stress in the 0° ply reaches the fiber failure stress first. Therefore, pull-out type failure follows. The stress-strain curve of the baseline specimen is plotted in Figure 10. To use the same methodology as Green et al. [1], failure (red dot) was taken as the first significant load drop (greater than 5%) on the load-displacement curve. The DPM runs on Abaqus/Explicit and mass scaling is used to mitigate the calculation durations. Oscillations on the stress/strain curves are a consequence of this. To make sure that the quasi-static nature of the phenomenon is still respected, the total kinetic energy is verified to be lower than 1% of the total internal energy. In addition to that, Figure 11 shows the different types of damage that occur when the laminate fails (red triangle on Figure 10): fiber failure in 0° ply; delaminated elements and matrix cracked elements in the laminate, for $t = 1\text{ mm}$, $d = 3.175\text{ mm}$ in baseline configuration. Pristine elements and totally damaged elements are colored in blue and red respectively. The red triangle represents the instant when this snapshot was taken. **The pull-out type of failure is correctly accounted for by the model since numerical failure patterns correlate well with experimental ones (Figure 3-Top left).**

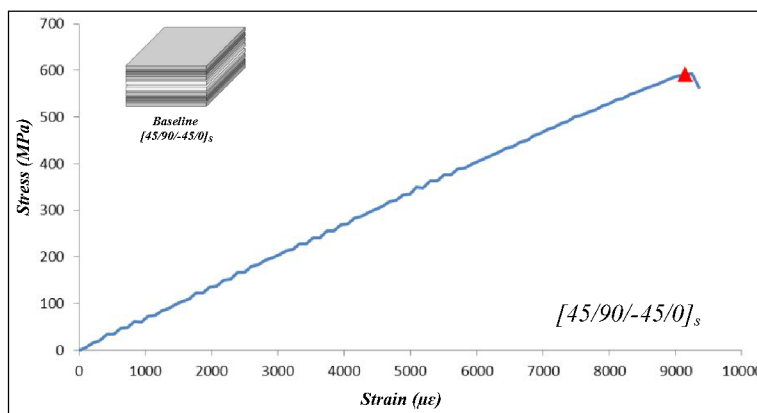
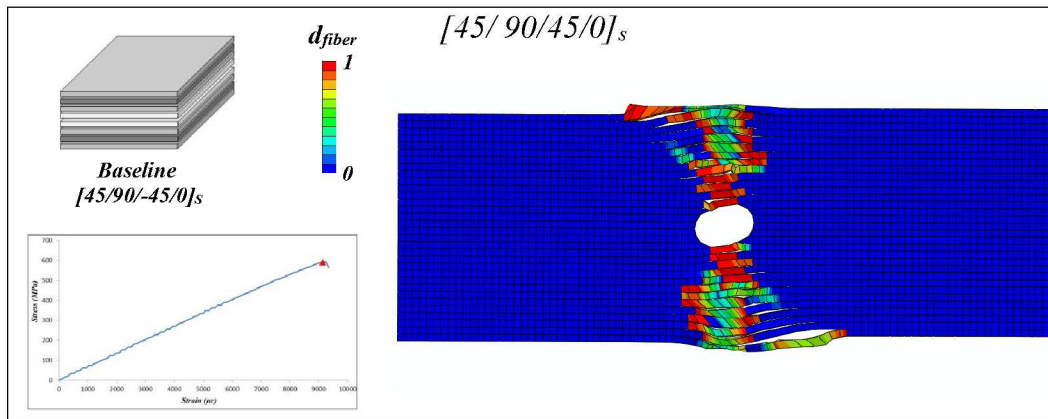
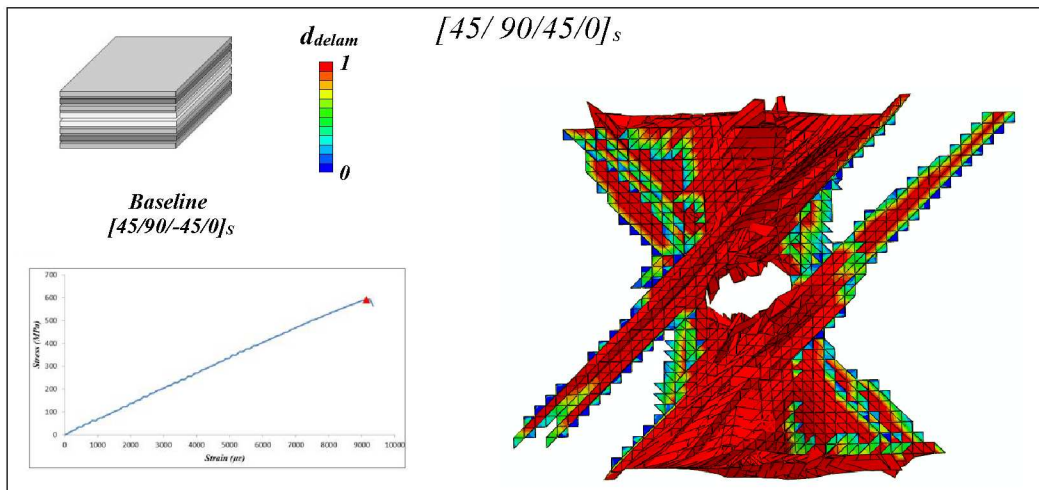


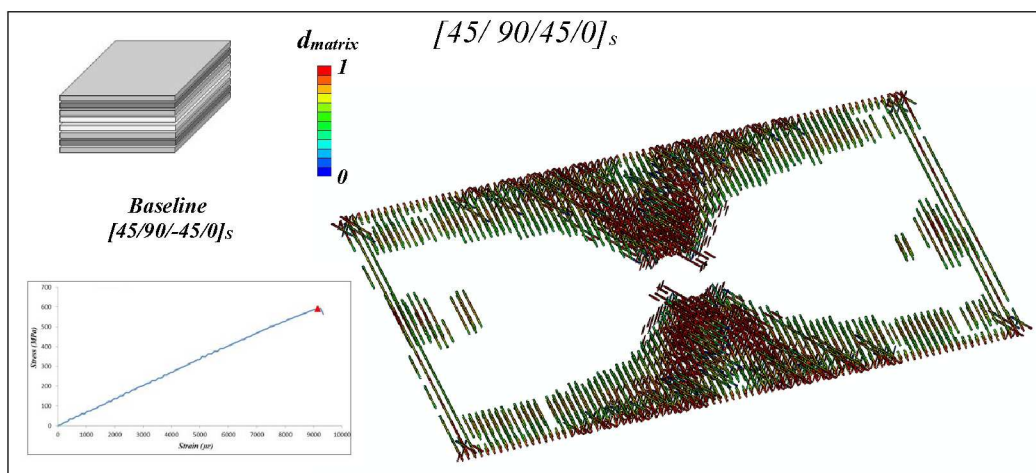
Figure 10. Stress-strain curve for $t = 1\text{ mm}$, $d = 3.175\text{ mm}$ for baseline configuration



-a-



-b-



-c-

53
54
55
56
57
58
59
60

Figure 11. a) Fiber failure in 0° ply, (b) Delaminated elements and (c) matrix cracked elements for $t = 1$ mm, $d = 3.175$ mm for baseline configuration

2. Ply-level scaling

The main failure mechanism observed when increasing the number of plies blocked together (ply-level scaled specimen) is delamination. Extensive delamination develops before fiber failure, even though there are some cases where a pull-out type failure occurs. The fact that plies are blocked together creates high interlaminar strength and triggers delamination.

This failure mechanism consists in an extensive delamination between -45° and 0° plies, accompanied by failure via splitting of the off-axis plies as shown in Figure 14. Splitting of the 0° ply also occurs and leaves two ligaments, one on either side of the hole to carry the load (Figure 14). Therefore there is no longer a stress concentration around the hole and the failure of 0° ply will occur on the free edges (Figure 15).

- **1D scaling effect**

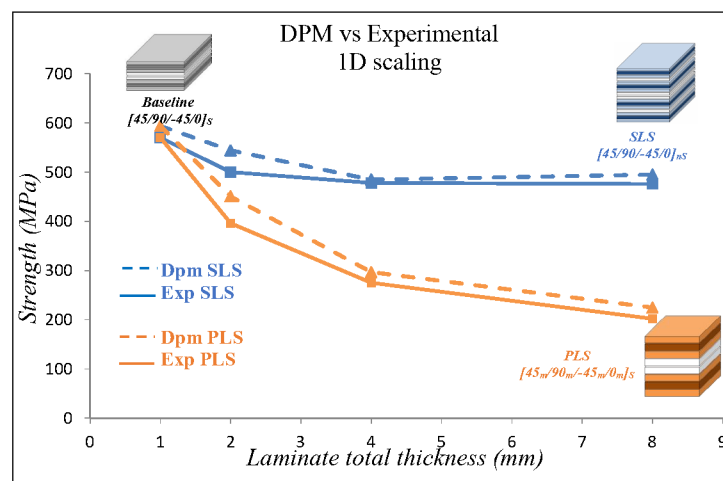


Figure 12. Experimental vs numerical strength with respect to ply thickness (1D scaling)

The numerically obtained curves of the 1D scaling routine are plotted in Figure 12. Increasing the thickness of a specimen with constant hole diameter leads to a decrease in failure stress. The evolution of the curve presented in this figure is representative of the classic thickness effect. It is due to the extra elastic energy stored in the blocked plies becoming available for delamination to propagate. There is more energy for delamination to propagate when the specimen is thicker, so more delamination when the number of interfaces between plies of different orientations is the same (6). Additionally, having thicker plies increases the interlaminar stress and therefore triggers delamination earlier. Similarly, there is more matrix cracking in thicker specimens. The thicker the specimen, the lower the apparent stress at failure.

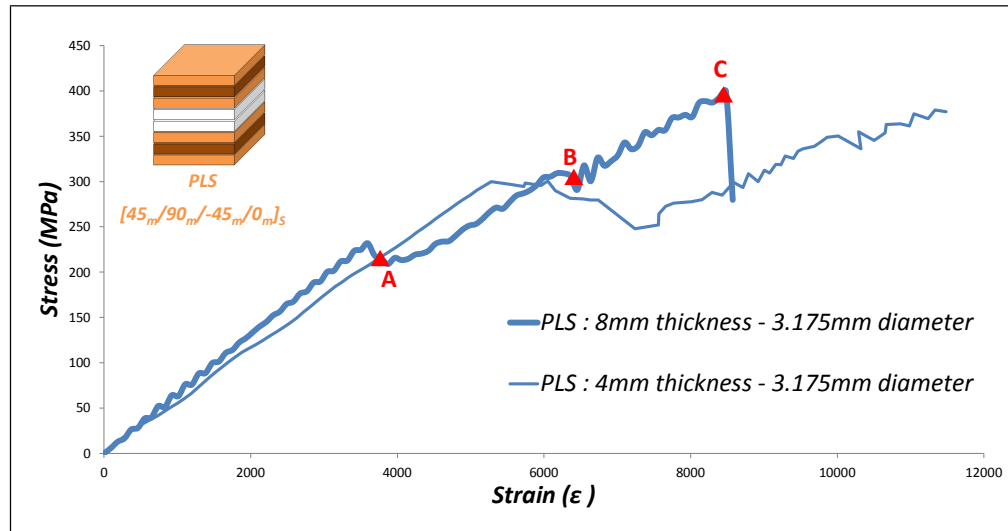


Figure 13. Stress-strain curve for $t = 4$ mm, $d = 3.175$ mm and for $t = 8$ mm, $d = 3.175$ mm in PLS configuration

The failure mechanisms of two specimens, at the same value of stress (a triangle marker at 210 MPa), are compared in Figure 13, where stress-strain curves are shown for $t = 4$ mm, $D = 3.175$ mm and $t = 8$ mm, $D = 3.175$ mm configurations. At this stress value, for the first configuration, there is only initiation of delamination and matrix cracking while, in the second one, the failure stress is already reached; delamination begins, accompanied by matrix cracking and splitting of the 0° ply. These damage mechanisms are displayed in Figure 14-a, Figure 14-c and Figure 14-e. The propagation of such damage in a delamination-type failure mode can be observed in Figure 14-b, Figure 14-d, Figure 14-f, and Figure 15. Very little fiber failure of the central ply is observed and the damaged (red) elements are mostly associated with a numerical failure close to the applied boundary conditions. The delamination type of failure is correctly accounted for by the model since numerical failure patterns correlate well with the experimental one (Figure 3-Bottom).

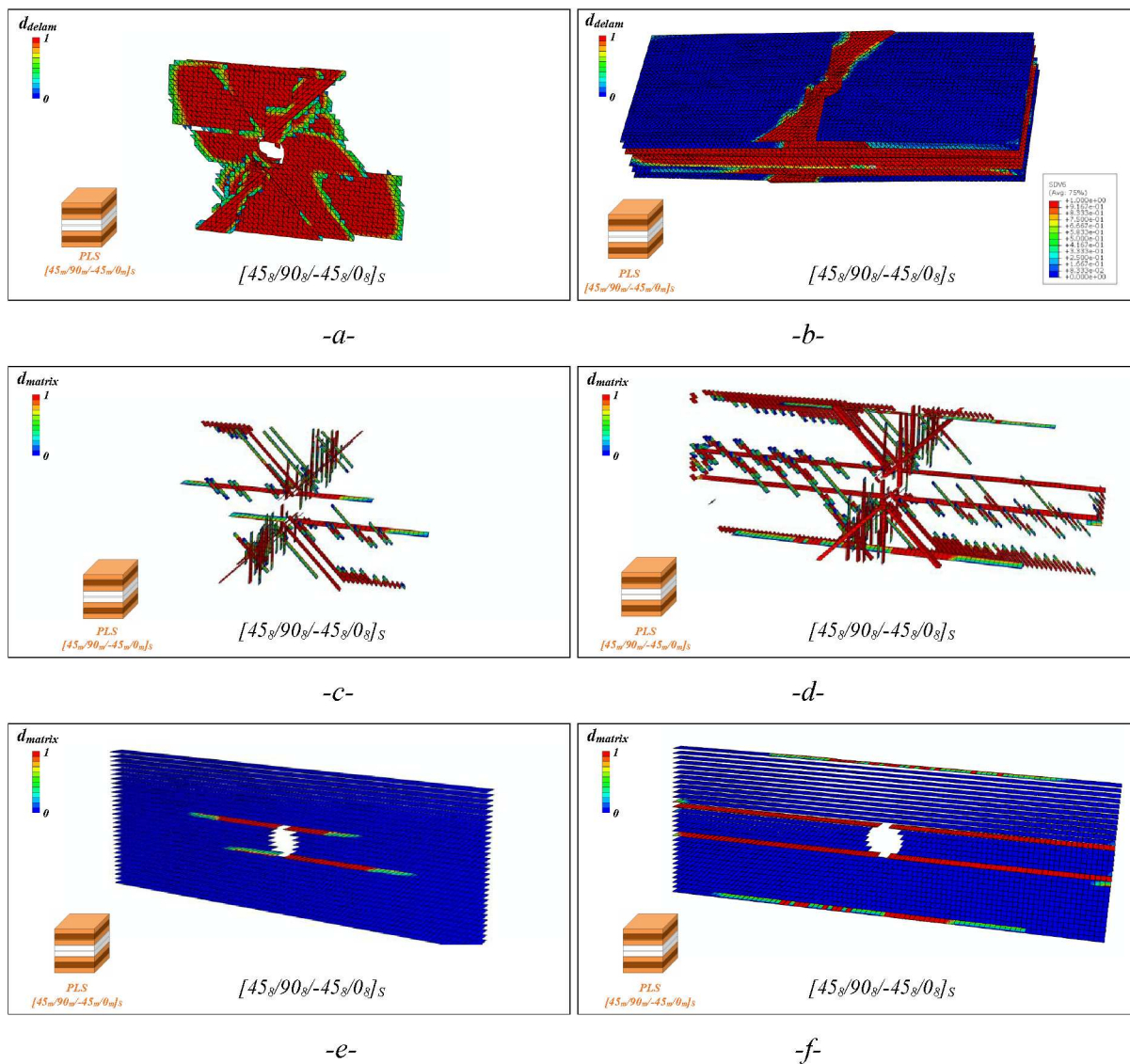


Figure 14. (a) delaminated elements, (c) matrix cracked elements and (e) splitting on 0° ply, at point A, and B (resp. b, d, f) for $t = 8$ mm, $d = 3.175$ mm for PLS configuration

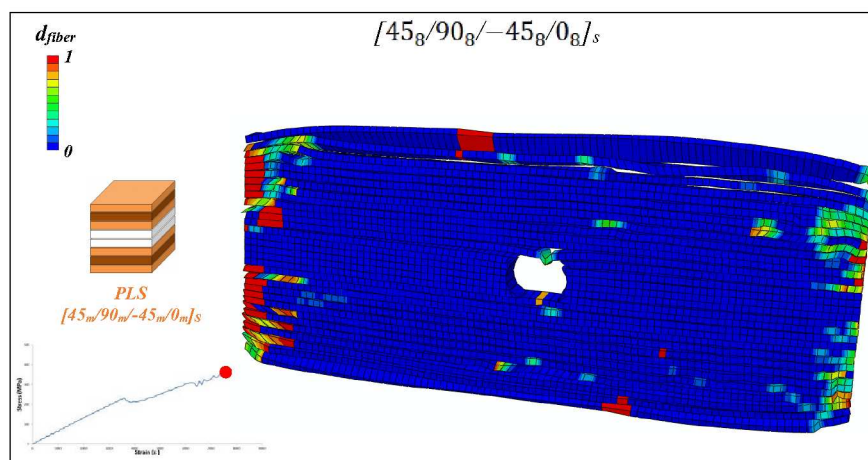


Figure 15. Fiber failure of 0° ply, at point C for $t = 8$ mm, $d = 3.175$ mm for PLS configuration

- **2D scaling effect**

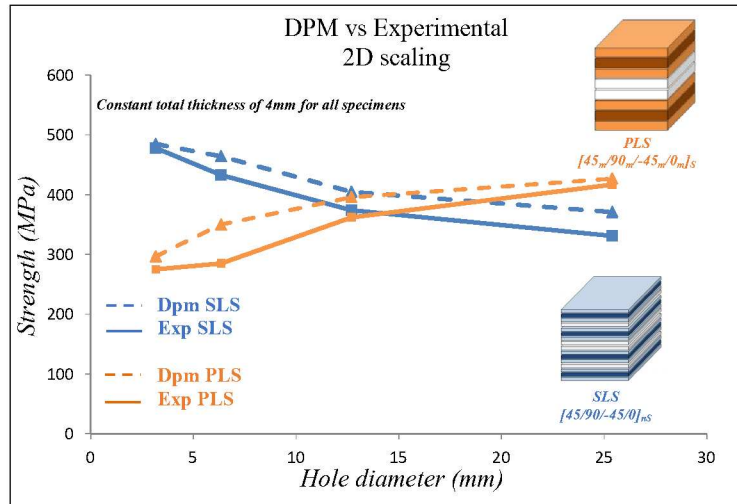


Figure 16. Experimental vs numerical strength with respect to hole diameter (2D scaling)

Figure 16 summarizes the evolution of strength for an increase of in-plane dimensions (2D scaling effect). On in-plane 2D, for the PLS specimen, opposite trends are identified for the effect of size on strength. Increasing hole diameter while keeping specimen thickness constant leads to an increase in failure stress, in opposition to what happens in 1D scaling. It is recalled that the 1D specimens failed by delamination as presented in Table 4.

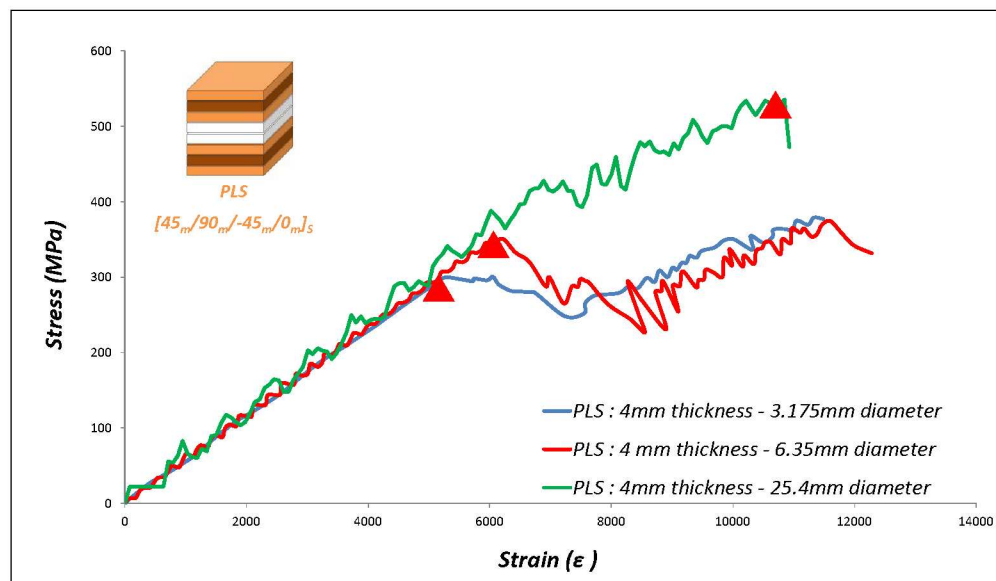


Figure 17. Stress-strain curves for $t = 4$ mm, $d = 3.175$, $d = 6.35$ and $d = 25.4$ mm in PLS configuration

The 4 mm thick specimens with several hole dimensions are compared in Figure 17 and Figure 18, which show the difference between stress-strain curve, delaminated elements, splitting and matrix cracked elements for a 4 mm thick laminate with 3.175 mm, 6.35 mm and 25.4 mm hole diameters.

The images presented in Figure 18 were taken at structural failure for each of the three configurations (represented by red triangles in Figure 17).

The stress at which delamination occurred increased from 300 MPa for a 4 mm thick laminate with a 3.175 mm hole diameter, to 425 MPa for a 4 mm thick laminate with a 25.4 mm hole diameter. As specimens fail by delamination, there is a discontinuity on stress-strain curves, and it can be seen in Figure 17 that load drops depend on the size of the hole. The smaller the hole is, the earlier the load drops take place. Load drops correspond to massive delaminations before 0° fiber failure but the stress value in the first load drop is always taken as failure even if it is not the maximum value of stress on the curve, as the specimen has delaminated extensively.

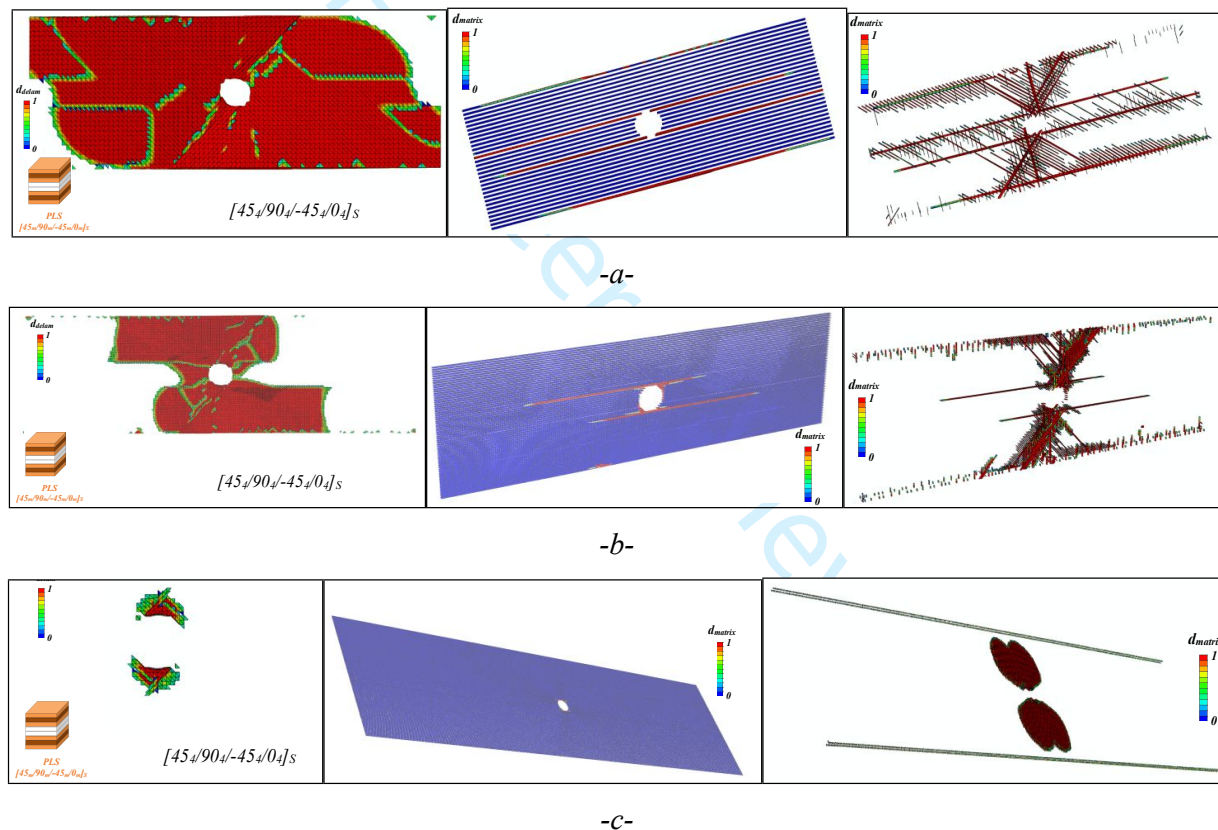


Figure 18. Delaminated elements, splitting on 0° ply and matrix cracked elements for $t = 4\text{ mm}$,
 (a) $d = 3.175\text{ mm}$, (b) $d = 6.35\text{ mm}$ and (c) $d = 25.4\text{ mm}$ in PLS configuration

Figure 18 shows the difference between delaminated elements according to the size of the hole. For a large hole, delamination is small, there is just initiation of splitting on the 0° ply, and matrix cracking just occurs around the hole boundary and free edges. For a smaller hole, delaminations are larger and accompanied by splitting, forming the extensive delamination. The extensive delamination on a smaller hole propagates quickly from the hole to the specimen edge and quickly reaches failure

stress. This will happen at lower stress for smaller holes. For larger holes, the stress at which the extensive delamination crosses the edge is higher; this is the reason for the increase in failure stress as hole diameter increases. This is not a classic size effect. The most delamination, matrix cracking and splitting in 0° ply is seen on the smaller hole.

The wider specimen failed at higher stress, as could be expected due to the greater difficulty of delamination propagating across the width. The larger the hole is, the wider the specimen is, and this is why the higher apparent stress at failure is seen on the larger hole.

- **3D scaling effect**

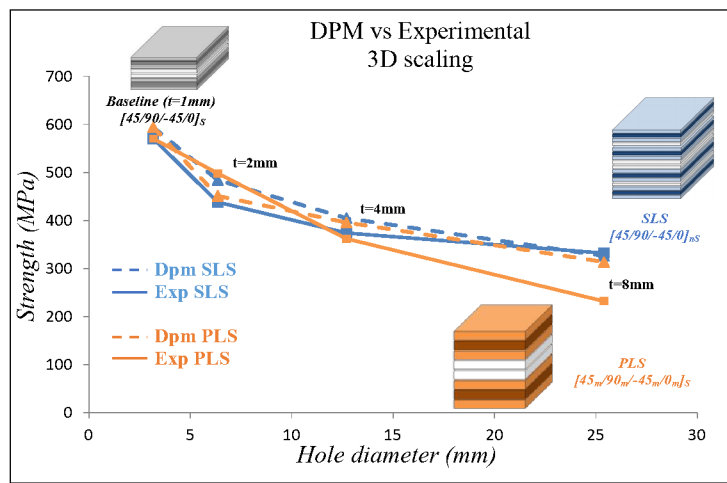


Figure 19. Experimental vs numerical strength with respect to hole diameter (3D scaling)

In 3D scaling (Figure 18), a decrease in failure strength is observed when both diameter and total thickness increase. This shows that, for PLS configurations, the effect of increasing thickness is dominant over the effect of increasing hole diameter.

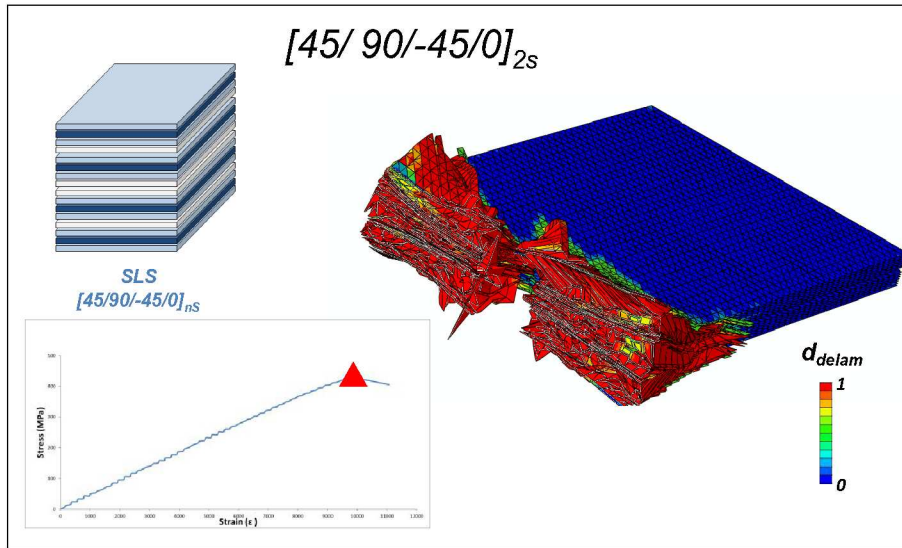
3. *Sublaminated level scaling*

In specimens with thickness increased by the sublaminated-level scaling method, fiber failure occurs first, with extensive pull-out on smaller specimens, as for the 2 mm thick laminate with 3.175 mm hole diameter shown in **Figure 20**, and more brittle failure occurs on larger specimens like the 4 mm thick laminate with 25.4 mm hole diameter, as shown in Figure 22 and **Figure 21**.

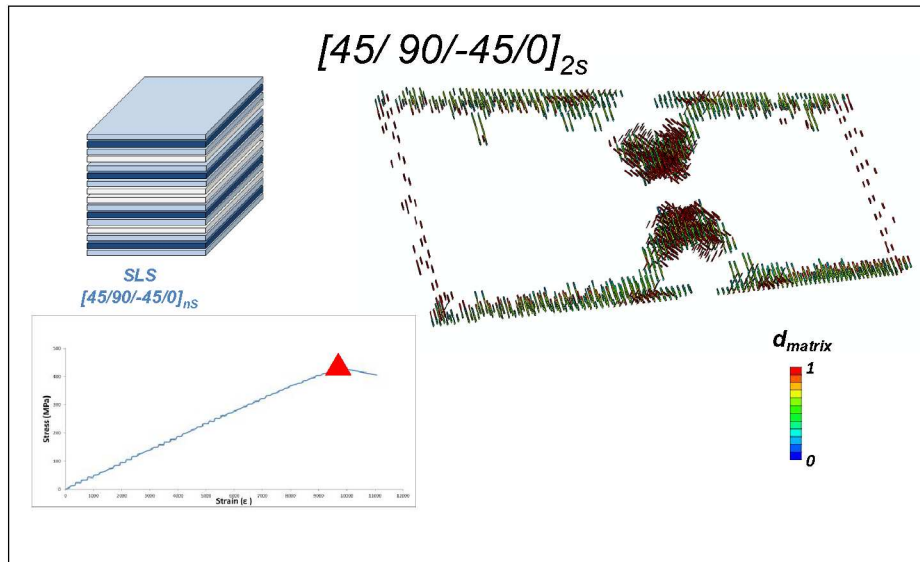
For pull-out type failure, the laminate failure is sudden and dominated by fiber failure, which triggers delamination while propagating. **Figure 20** represents a typical stress-strain curve for a 2 mm thick sublaminated-level scaled specimen with a 3.175 mm diameter hole. It is seen that the stress-strain curve increases linearly and ends suddenly when the fiber failure occurs. In the pull-out failure mechanism, fiber failure within the 0° plies is accompanied by delamination between some of the off-axis plies. Depending on the thickness of the laminate, this delamination occurs on plies close to the surface or across the entire thickness of the specimen (**Figure 20-a**). Matrix cracking is observed in several plies, essentially on 90° plies, crossing from the hole edge to free edges (**Figure 20-b**). Matrix cracking on off-axis plies is just located around the hole, in the initiation phase.

Brittle failure has a mechanism similar to that of pull-out type failure; it is fiber-dominated. **Figure 21** represents a typical stress-strain curve for a 4 mm thick sublaminated-level scaled specimen with a 12.7 mm diameter hole. The stress-strain curve is seen to increase linearly and ends when the fiber failure occurs. The failure begins from matrix cracking with delamination in all plies and then fiber failure in the 0° ply appears as shown in **Figure 21**. For fiber failure and delamination between -45°/0° ply, failure occurs on the edge of the hole, and then propagates adjacent to the hole, creating a clean fracture surface across the width of the specimen, at the mid-plane of the laminate. The fracture plane is the same in every ply of the laminate. Matrix cracking begins around the hole and then extends only on the free edges, due to the 90° plies (Figure 22). The failure scenario is similar to that of pull-out failure but with less damage (matrix cracks and delamination) extension before total failure. **The brittle type of failure is correctly accounted for by the model since numerical failure patterns correlate well with experimental ones (Figure 3-Top right).**

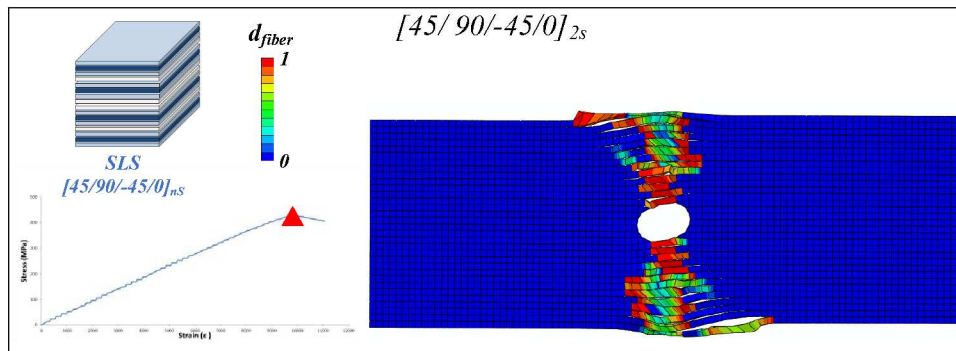
Increasing the laminate thickness by using extra sublaminaes, from 4 mm to 8 mm, does not change the failure stress value significantly, as seen the 1D scaling results (Figure 16). This means that strength is globally independent of thickness. Increasing the thickness of the specimens by increasing the number of sublaminaes results in distribution of 0° plies throughout the thickness. **Therefore, the 0° plies have the capacity to arrest propagation of the sub-critical damage, and confine it to the two outermost sublaminaes.**



-a-



-b-



-c-

53
54
55
56
57
58
59

Figure 20. (a) Delamination across the width, (b) matrix cracked elements and (c) fiber failure in 0° ply , for $t = 2$ mm, $d = 3.175$ mm in SLS configuration

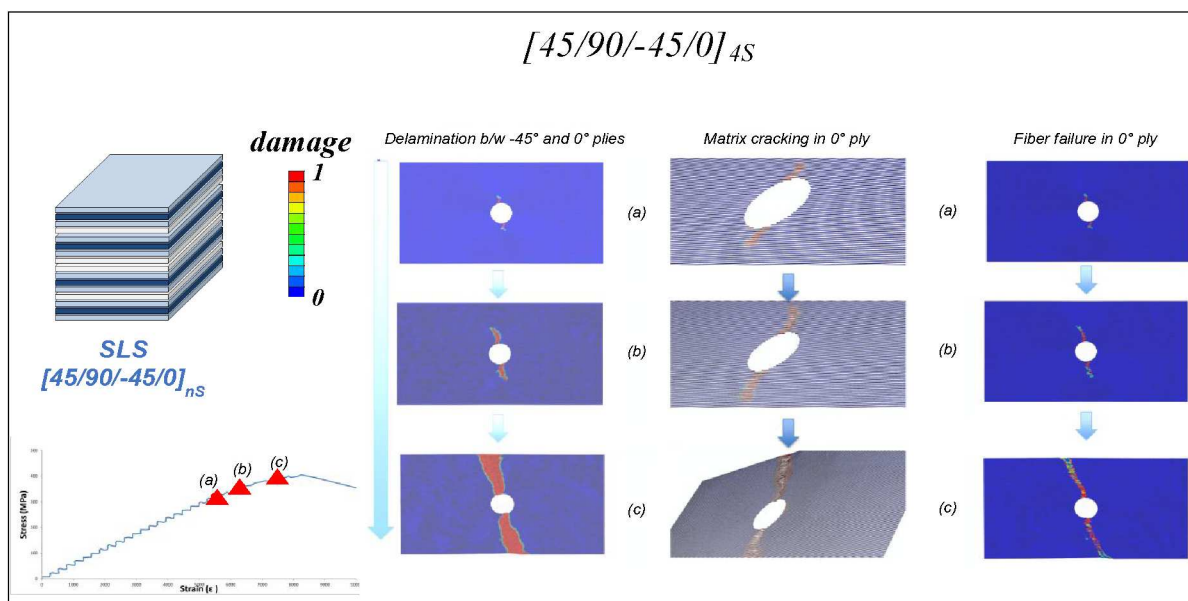


Figure 21. Delamination, Matrix cracking and fiber failure for $t = 4$ mm, $d = 12.7$ mm for SLS configuration

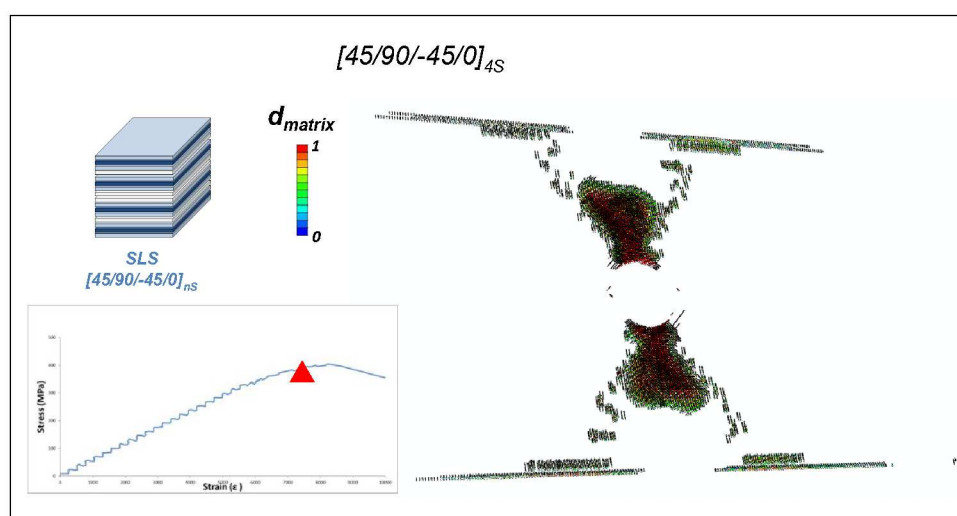


Figure 22. Matrix cracked elements, for $t = 4$ mm, $d = 12.7$ mm for SLS configuration

In all cases of scaling routines (one-, two- and three-dimensionnal scaling), it can be seen (Figure 12, Figure 16, and Figure 19) that increasing size leads to a decrease in failure stress, which becomes asymptotic at large sizes. The thickness effect (1D - Figure 12) is very small compared to the effect of hole size (2D - Figure 16). The larger the hole, the lower the value of strength. This is because these specimens generally fail by fiber failure. For this type of failure mechanism, extensive delamination at the hole edge appears after fiber failure, so splitting in 0° plies is also delayed for a larger hole (reducing the stress distribution) and results in failure of the specimen at a lower stress.

4. Comparison between PLS and SLS

1 The curves obtained experimentally and numerically are plotted in Figure 12, Figure 16, and
2 Figure 19, respectively, for 1D, 2D and 3D scaling. Good experiment-model correlation can be
3 observed. However, the numerical results exhibit slightly higher failure stresses than the associated
4 experimental results. The 1D scaling curve represents the variation of the strength as a function of
5 the thickness. It can be seen that, when the total thickness of the laminate increases, the failure stress
6 is much higher for SLS configurations than for PLS ones. The effect of ply thickness is much
7 stronger in PLS than in SLS because the failure mechanism of laminates in PLS is delamination,
8 while SLS laminates fail by pull-out or by brittle-type failure. Increasing the ply thickness in PLS
9 laminates leads to fast delamination and this phenomenon affects the strength of the structure
10 negatively. The 2D scaling curve is less straightforward. The reader will recognize a classical size-
11 effect curve for the SLS configurations whereas the PLS ones exhibit a counter-intuitive increase of
12 the failure stress when the hole diameter increases. This is due to the grouping of plies, which favors
13 delamination. Indeed, delamination saves the specimen by delaying fiber failure. In 3D scaling, both
14 configurations show a decrease in failure strength when the hole diameter increases. Thus, for PLS,
15 the effect of increasing total thickness is dominant over the effect of increasing hole diameter. There
16 is no significant difference between PLS and SLS, so, in the end, the classical size effect is seen:
17 increasing the diameter of the hole leads to a decrease in the strength.
18
19
20
21
22
23
24
25
26
27
28
29
30
31

32 The final fitting curves for the SLS and PLS configurations are presented in **Figure 23**. The black
33 curve represents the baseline, which is both PLS and SLS. **The blue and black curves represent
34 the SLS specimens, in which the main failure mechanisms are pull-out failure or brittle type
35 failure.** The effect of the hole diameter on the strength is quite logical: increasing hole diameter
36 leads to a decrease in strength. Whatever the thickness of the laminate or the diameter of the hole, the
37 strength decreases with the thickness and the size of the hole. **On the other hand, the PLS
38 variation of strength is less straightforward. This is due to the fact that failure is
39 predominantly influenced by delamination. It is also seen that PLS specimens have a different
40 behavior below and above a thickness of 2 mm.** The PLS effect follows the same logic as the SLS
41 for thicknesses from 1 mm to 2 mm. Then, when the thickness increases from 2 mm onwards, the PLS
42 effect is positive: increasing hole diameter leads to an increase of strength. This is due to the
43 grouping of plies, which favors delamination, then delamination saves the specimen and delays the
44 fiber failure. This thickness effect is beneficial at the beginning for large diameters but becomes
45 catastrophic, with a very large drop of strength, when too many plies are grouped. This can be
46 explained by the beneficial effect of grouping some plies together to promote delamination.
47 However, the use of this effect should not be exaggerated: if the laminate is too thick, early
48 delamination occurs and this is detrimental.
49
50
51
52
53
54
55
56
57
58
59
60

Depending on the thickness/hole diameter combination, the most beneficial choice in terms of failure stress varies. According to Figure 23, for laminate thicknesses of less than 2 mm, it seems better to use an SLS configuration when hole diameters are smaller than 5.7 mm (A) and PLS otherwise. For laminate thicknesses between 2 and 4 mm, it seems better to use an SLS configuration when hole diameter is smaller than 8.5 mm (B) and PLS otherwise. For thicker laminates, SLS seems to be the best candidate for all hole diameters (up to 25.4mm). Globally, the thicker the laminate is, the more appropriate the SLS configuration seems to be.

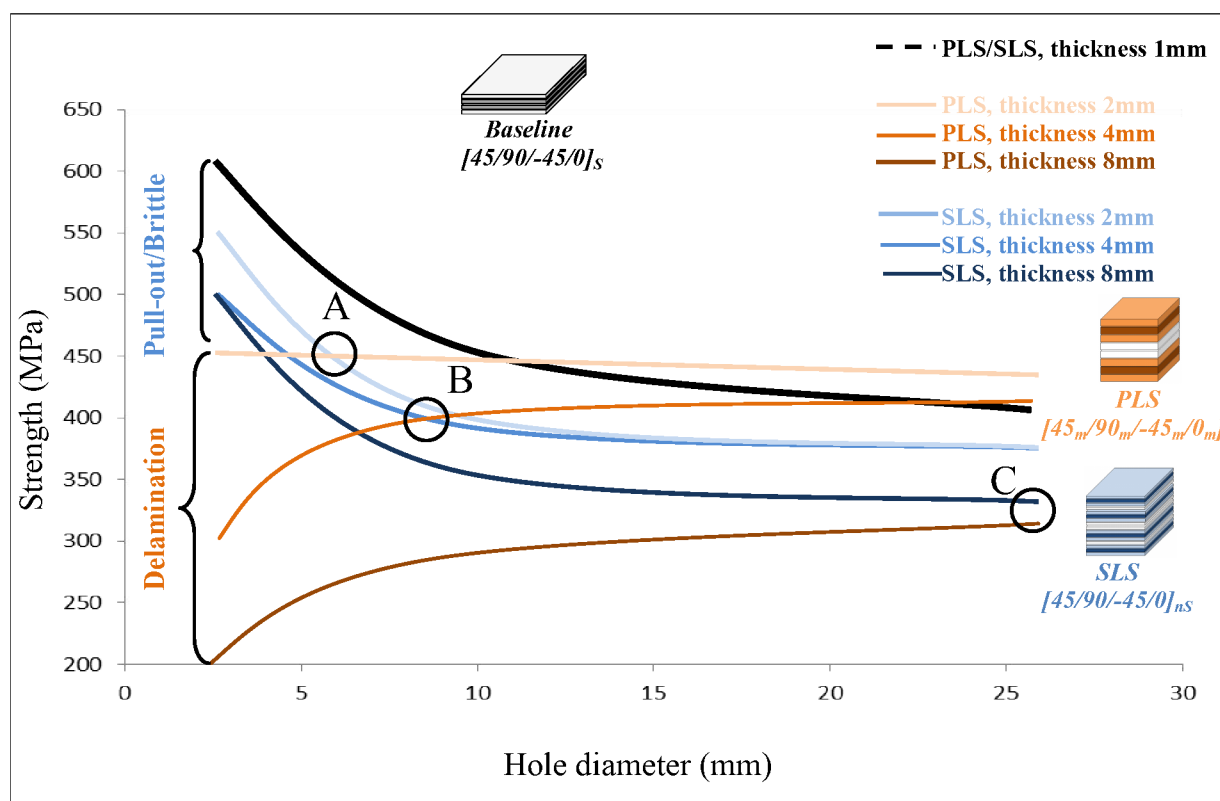


Figure 23. Fitting curves for PLS and SLS configurations

V. Conclusion

A comprehensive numerical framework has been presented whereby user-defined volume and cohesive element formulations have been developed to simulate the scaling effects acting on open hole tension tests. This has been achieved by taking the three main failure modes in laminated composites into account: matrix cracking, delamination and fiber failure. A specific meshing methodology has been used to allow for natural coupling between matrix cracks and delamination openings. The Discrete Ply Model needs a small number of parameters, all of which come from material tests. No numerical tuning parameter has been used.

The numerical framework has been validated against a large set of experimental data. Three types of scaling (1D, 2D and 3D) have been studied on two types of stacking sequences (Sublaminar-level and Ply-level scaling). The 3 types of failure (brittle, pull-out and delamination) observed experimentally have been correctly simulated. Consistent average failure stress values and evolutions have been observed according to various scaling methodologies.

Since the numerical results correlate well with the experimental observations, it can be considered that the DPM has been validated for evaluation of the failure of open hole tensile tests. This model has therefore been used to open up the field of investigations and simulate configurations not previously tested experimentally. Numerical simulations have been performed for all laminate thicknesses, from 1 mm to 8 mm, and for all hole diameters, from 3.175 mm to 25.4 mm. The idea is to provide charts to help engineers choose the best stacking sequence configuration between PLS and SLS for a given laminate thickness/hole diameter combination. Globally, the thicker the laminate is, the more suitable the SLS configuration seems to be. However, in some specific combinations (small thickness/small diameter hole), PLS can be a smarter choice.

It should be noted that the research presented in this article draws this conclusion for a specific type of material, stacking sequence and loading. Other combinations could lead to different behaviors and conclusions. It would be interesting to use the Discrete Ply Model to simulate a large number of cases, with different stacking sequences and compare the influence of stacking sequence with the hole and thickness effects. Moreover, the laminate has been studied in pure tension and it would be of interest to see whether the conclusions hold under multiaxial loadings.

Acknowledgment

The authors would like to express their gratitude to CALMIP (CALcul en Midi-Pyrénées, (<https://www.calmip.univ-toulouse.fr>) for access to the HPC resources under allocation p1026.

References

- [1] B. G. Green, M. R. Wisnom, and S. R. Hallett, 'An experimental investigation into the tensile strength scaling of notched composites', *Composites Part A: Applied Science and Manufacturing*, vol. 38, no. 3, pp. 867–878, Mar. 2007, doi: 10.1016/j.compositesa.2006.07.008.
- [2] Z. Bazant, *Scaling of Structural Strength*. Elsevier, 2005. doi: 10.1016/B978-0-7506-6849-1.X5000-7.
- [3] Z. P. Bazant, I. M. Daniel, and Z. Li, 'Size Effect and Fracture Characteristics of Composite Laminates', *Journal of Engineering Materials and Technology*, vol. 118, no. 3, pp. 317–324, Jul. 1996, doi: 10.1115/1.2806812.
- [4] M. R. Wisnom, S. R. Hallett, and C. Soutis, 'Scaling Effects in Notched Composites', *Journal of Composite Materials*, vol. 44, no. 2, pp. 195–210, Jan. 2010, doi: 10.1177/0021998309339865.
- [5] X. Xu, M. R. Wisnom, Y. Mahadik, and S. R. Hallett, 'An experimental investigation into size effects in quasi-isotropic carbon/epoxy laminates with sharp and blunt notches', *Composites Science and Technology*, vol. 100, pp. 220–227, Aug. 2014, doi: 10.1016/j.compscitech.2014.06.002.
- [6] P. P. Camanho, P. Maimí, and C. G. Dávila, 'Prediction of size effects in notched laminates using continuum damage mechanics', *Composites Science and Technology*, vol. 67, no. 13, pp. 2715–2727, Oct. 2007, doi: 10.1016/j.compscitech.2007.02.005.
- [7] S. R. Hallett, B. G. Green, W. G. Jiang, and M. R. Wisnom, 'An experimental and numerical investigation into the damage mechanisms in notched composites', *Composites Part A: Applied Science and Manufacturing*, vol. 40, no. 5, Art. no. 5, May 2009, doi: 10.1016/j.compositesa.2009.02.021.
- [8] K.-Y. Lin, *Fracture of filamentary composite materials*. 1977.
- [9] C. Harris and D. Morris, 'Role of Delamination and Damage Development on the Strength of Thick Notched Laminates', in *Delamination and Debonding of Materials*, W. Johnson, Ed. 100 Barr Harbor Drive, PO Box C700, West Conshohocken, PA 19428-2959: ASTM International, 1985, pp. 424-424–24. doi: 10.1520/STP36318S.
- [10] R. S. Vaidya, J. C. Klug, and C. T. Sun, 'Effect of Ply Thickness on Fracture of Notched Composite Laminates', *AIAA Journal*, vol. 36, no. 1, pp. 81–88, Jan. 1998, doi: 10.2514/2.355.
- [11] P. Lagace, 'Notch Sensitivity and Stacking Sequence of Laminated Composites', Philadelphia, 1986. Accessed: Jan. 19, 2022. [Online]. Available: <https://www.astm.org/stp35347s.html>
- [12] K.-Y. Chang, S. Llu, and F.-K. Chang, 'Damage Tolerance of Laminated Composites Containing an Open Hole and Subjected to Tensile Loadings', *Journal of Composite Materials*, vol. 25, no. 3, pp. 274–301, Mar. 1991, doi: 10.1177/002199839102500303.
- [13] J. M. Whitney and R. J. Nuismer, 'Stress Fracture Criteria for Laminated Composites Containing Stress Concentrations', *Journal of Composite Materials*, pp. 253–265, 1974.
- [14] J. Wang, P. J. Callus, and M. K. Bannister, 'Experimental and numerical investigation of the tension and compression strength of un-notched and notched quasi-isotropic laminates', *Composite Structures*, vol. 64, no. 3, pp. 297–306, Jun. 2004, doi: 10.1016/j.compstruct.2003.08.012.
- [15] J. Awerbuch and M. S. Madhukar, 'Notched Strength of Composite Laminates: Predictions and Experiments—A Review', *Journal of Reinforced Plastics and Composites*, vol. 4, no. 1, pp. 3–159, Jan. 1985, doi: 10.1177/073168448500400102.
- [16] J. W. Mar and K. Y. Lin, 'Fracture mechanics correlation for tensile failure of filamentary composites with holes', *Journal of Aircraft*, vol. 14, no. 7, pp. 703–704, Jul. 1977, doi: 10.2514/3.44618.
- [17] A. Sova, 'Fracture toughness of boron/aluminium laminates with various proportions of 0 and +/-45° plies', NASA technical paper, 1980.
- [18] R. F. Karlak, 'Hole effects in a related series of symmetrical laminates', in *Proceedings of the Fourth Joint ASM-Metallurgical Society of AIME Symposium on Failure Modes in Composites, 1977*, 1977, pp. 105–117.
- [19] R. B. Pipes, R. C. Wetherhold, and J. W. Gillespie Jr, 'Notched strength of composite materials', *Journal of Composite Materials*, vol. 13, no. 2, pp. 148–160, 1979.

- [20] R. B. Pipes, J. W. Gillespie Jr., and R. C. Wetherhold, 'Superposition of the notched strength of composite laminates', *Polymer Engineering & Science*, vol. 19, no. 16, pp. 1151–1155, 1979, doi: 10.1002/pen.760191604.
- [21] R. B. Pipes, R. C. Wetherhold, and J. W. Gillespie Jr, 'Macroscopic fracture of fibrous composites', *Materials Science and Engineering*, vol. 45, no. 3, pp. 247–253, 1980.
- [22] C. Hochard, N. Lahellec, and C. Bordreuil, 'A ply scale non-local fibre rupture criterion for CFRP woven ply laminated structures', *Composite Structures*, vol. 80, no. 3, p. 321, 2007.
- [23] P. P. Camanho, G. H. Erçin, G. Catalanotti, S. Mahdi, and P. Linde, 'A finite fracture mechanics model for the prediction of the open-hole strength of composite laminates', *Composites Part A: Applied Science and Manufacturing*, vol. 43, no. 8, pp. 1219–1225, Aug. 2012, doi: 10.1016/j.compositesa.2012.03.004.
- [24] D. Leguillon, D. Quesada, C. Putot, and E. Martin, 'Prediction of crack initiation at blunt notches and cavities – size effects', *Engineering Fracture Mechanics*, vol. 74, pp. 2420–2436, Oct. 2007, doi: 10.1016/j.engfracmech.2006.11.008.
- [25] Y. Mohammed, M. K. Hassan, H. A. E.- Ainin, and A. M. Hashem, 'Size effect analysis of open-hole glass fiber composite laminate using two-parameter cohesive laws', *Acta Mechanica*, vol. 226, no. 4, pp. 1027–1027, Apr. 2015.
- [26] D. S. Dugdale, 'Yielding of steel sheets containing slits', *Journal of the Mechanics and Physics of Solids*, vol. 8, no. 2, pp. 100–104, May 1960, doi: 10.1016/0022-5096(60)90013-2.
- [27] G. I. Barenblatt, 'The Mathematical Theory of Equilibrium Cracks in Brittle Fracture', in *Advances in Applied Mechanics*, vol. 7, H. L. Dryden, Th. von Kármán, G. Kuerti, F. H. van den Dungen, and L. Howarth, Eds. Elsevier, 1962, pp. 55–129. doi: 10.1016/S0065-2156(08)70121-2.
- [28] P. Camanho and S. Hallett, *Numerical Modelling of Failure in Advanced Composite Materials*, 1er édition. Woodhead Publishing, 2015.
- [29] B. Y. Chen, T. E. Tay, P. M. Baiz, and S. T. Pinho, 'Numerical analysis of size effects on open-hole tensile composite laminates', *Composites Part A: Applied Science and Manufacturing*, vol. 47, pp. 52–62, Apr. 2013, doi: 10.1016/j.compositesa.2012.12.001.
- [30] E. Abisset, F. Daghia, and P. Ladevèze, 'On the validation of a damage mesomodel for laminated composites by means of open-hole tensile tests on quasi-isotropic laminates', *Composites Part A: Applied Science and Manufacturing*, vol. 42, no. 10, pp. 1515–1524, Oct. 2011, doi: 10.1016/j.compositesa.2011.07.004.
- [31] F. Laurin, N. Carrere, C. Huchette, and J.-F. Maire, 'A multiscale hybrid approach for damage and final failure predictions of composite structures', *Journal of Composite Materials*, vol. 47, no. 20–21, Art. no. 20–21, Sep. 2013, doi: 10.1177/0021998312470151.
- [32] M. Ridha, C. H. Wang, B. Y. Chen, and T. E. Tay, 'Modelling complex progressive failure in notched composite laminates with varying sizes and stacking sequences', *Composites Part A: Applied Science and Manufacturing*, vol. 58, pp. 16–23, Mar. 2014, doi: 10.1016/j.compositesa.2013.11.012.
- [33] N. Hongkarnjanakul, 'Modélisation numérique pour la tolérance aux dommages', 2013.
- [34] X. Xu, M. R. Wisnom, X. Li, and S. R. Hallett, 'A numerical investigation into size effects in centre-notched quasi-isotropic carbon/epoxy laminates', *Composites Science and Technology*, vol. 111, pp. 32–39, May 2015, doi: 10.1016/j.compscitech.2015.03.001.
- [35] M. R. Wisnom, 'Modelling discrete failures in composites with interface elements', *Composites Part A: Applied Science and Manufacturing*, vol. 41, no. 7, pp. 795–805, Jul. 2010, doi: 10.1016/j.compositesa.2010.02.011.
- [36] W.-G. Jiang, S. Hallett, B. Green, and M. Wisnom, 'A concise interface constitutive law for analysis of delamination and splitting in composite materials and its application to scaled notched tensile specimens', *International Journal for Numerical Methods in Engineering*, vol. 69, pp. 1982–1995, Feb. 2007, doi: 10.1002/nme.1842.
- [37] M. J. Swindeman, E. V. Iarve, R. A. Brockman, D. H. Mollenhauer, and S. R. Hallett, 'Strength Prediction in Open Hole Composite Laminates by Using Discrete Damage Modeling', *AIAA Journal*, vol. 51, no. 4, pp. 936–945, Apr. 2013, doi: 10.2514/1.J051773.
- [38] B. Chen, T. E. Tay, S. Pinho, and V. B. C. Tan, 'Modelling the tensile failure of composites with the floating node method', *Computer Methods in Applied Mechanics and Engineering*, vol. 308, Jun. 2016, doi: 10.1016/j.cma.2016.05.027.
- [39] H. Bao and G. Liu, 'Progressive failure analysis on scaled open-hole tensile composite laminates', 2016, doi: 10.1016/J.COMPSTRUCT.2016.05.017.
- [40] R. Higuchi, T. Okabe, and T. Nagashima, 'Numerical simulation of progressive damage and failure in composite laminates using XFEM/CZM coupled approach', *Composites Part A: Applied Science and Manufacturing*, vol. 95, pp. 197–207, Apr. 2017, doi: 10.1016/j.compositesa.2016.12.026.

- [41] M. W. Joosten, Q. D. Yang, M. Blacklock, and C. H. Wang, 'A cohesive network approach for modelling fibre and matrix damage in composite laminates', *Composite Structures*, vol. 206, pp. 658–667, Dec. 2018, doi: 10.1016/j.compstruct.2018.08.087.
- [42] X. Lu, M. Ridha, V. B. C. Tan, and T. E. Tay, 'Adaptive Discrete-Smeared Crack (A-DiSC) Model for Multi-Scale Progressive Damage in Composites', *Composites*, 2019, Accessed: Jan. 20, 2022. [Online]. Available: <https://10.1016/j.compositesa.2019.105513>
- [43] C. Bouvet, B. Castanié, M. Bizeul, and J.-J. Barrau, 'Low velocity impact modelling in laminate composite panels with discrete interface elements', *International Journal of Solids and Structures*, vol. 46, no. 14–15, pp. 2809–2821, Jul. 2009, doi: 10.1016/j.ijsolstr.2009.03.010.
- [44] C. Bouvet, S. Rivallant, and J. J. Barrau, 'Low velocity impact modeling in composite laminates capturing permanent indentation', *Composites Science and Technology*, vol. 72, no. 16, pp. 1977–1988, Nov. 2012, doi: 10.1016/j.compscitech.2012.08.019.
- [45] S. Rivallant, C. Bouvet, and N. Hongkarnjanakul, 'Failure analysis of CFRP laminates subjected to compression after impact: FE simulation using discrete interface elements', *Composites Part A: Applied Science and Manufacturing*, vol. 55, pp. 83–93, Dec. 2013, doi: 10.1016/j.compositesa.2013.08.003.
- [46] L. Adam, C. Bouvet, B. Castanié, A. Daidié, and E. Bonhomme, 'Discrete ply model of circular pull-through test of fasteners in laminates', *Composite Structures*, vol. 94, no. 10, pp. 3082–3091, Oct. 2012, doi: 10.1016/j.compstruct.2012.05.008.
- [47] V. Achard, C. Bouvet, B. Castanié, and C. Chirol, 'Discrete ply modelling of open hole tensile tests', *Composite Structures*, vol. 113, pp. 369–381, Jul. 2014, doi: 10.1016/j.compstruct.2014.03.031.
- [48] J. Serra, C. Bouvet, B. Castanié, and C. Petiot, 'Scaling effect in notched composites: The Discrete Ply Model approach', *Composite Structures*, vol. 148, pp. 127–143, Jul. 2016, doi: 10.1016/j.compstruct.2016.03.062.
- [49] 'Hexcel 8552, Epoxy Matrix Product Datasheet. pdf download from: <http://www.hexcelcomposites.com/Markets/Products/Prepregs/PrepregDownld.html> (Last viewed: 26/08/05).'
- [50] J. Serra, C. Bouvet, B. Castanié, and C. Petiot, 'Experimental and numerical analysis of Carbon Fiber Reinforced Polymer notched coupons under tensile loading', *Composite Structures*, vol. 181, pp. 145–157, Dec. 2017, doi: 10.1016/j.compstruct.2017.08.090.
- [51] J. Serra, J. E. Pierré, J. C. Passieux, J. N. Périé, C. Bouvet, and B. Castanié, 'Validation and modeling of aeronautical composite structures subjected to combined loadings: The VERTEX project. Part 1: Experimental setup, FE-DIC instrumentation and procedures', *Composite Structures*, vol. 179, pp. 224–244, Nov. 2017, doi: 10.1016/j.compstruct.2017.07.080.
- [52] N. Li and P. H. Chen, 'Micro–macro FE modeling of damage evolution in laminated composite plates subjected to low velocity impact', *Composite Structures*, vol. 147, pp. 111–121, Jul. 2016, doi: 10.1016/j.compstruct.2016.02.063.